A FEM-based model to predict the behaviour of RC beams shear strengthened according to the NSM technique

Joaquim A. O. Barros [1], Hadi Baghi [2], Salvador J. E. Dias [3], A. Ventura-Gouveia [4]

[1]Full Prof., ISISE, Dep. Civil Eng., Minho University, Guimarães, Portugal, barros@civil.uminho.pt, corresponding Author

[2]PhD Candidate, Dep. Civil Eng., Minho University, Guimarães, Portugal, hadibaghi@gmail.com

[3]Assistant Prof., ISISE, Dep. Civil Eng., Minho University, Guimarães, Portugal, sdias@civil.uminho.pt

[4]Adjunct Prof., ISISE, Dep. Civil Eng., School of Technology and Management of Viseu, Viseu, Portugal, ventura@estv.ipv.pt

Abstract

Experimental research has demonstrated the excellent performance of the near surface mounted (NSM) technique with carbon fibre reinforced polymer (CFRP) laminates for the shear strengthening of reinforced concrete (RC) beams. This paper presents a finite element analysis to evaluate the behaviour of RC beams shear strengthened with NSM CFRP laminates. To predict correctly the deformational and the cracking behaviour of RC elements failing in shear using a smeared crack approach, the strategy adopted to simulate the crack shear stress transfer is crucial. For this purpose, a strategy for modelling the fracture mode II was implemented in a smeared crack model already existing in the FEM-based computer program, FEMIX. This strategy is mainly based on a softening shear stress-shear strain diagram adopted for modelling the crack shear stress transfer.

To assess the predictive performance of the developed model, the experimental tests carried out with a series of T cross section RC beams shear strengthened according to the NSM technique by using CFRP laminates were simulated. In this series of beams, three different percentages of CFRP laminates and, for each CFRP percentage, three inclinations for the laminates were tested: 90º, 60º and 45º. By using the properties obtained from the experimental program for the characterization of the relevant properties of the intervening materials, and deriving from inverse analysis the data for the crack shear softening diagram, the simulations carried out have fitted with high accuracy the deformational and cracking behaviour of the

tested beams, as well as the strain fields in the reinforcements. The constitutive model is briefly described, and the simulations are presented and analysed.

Keywords: CFRP; NSM; shear strengthening; FEM; material nonlinear analysis.

1. INTRODUCTION

Near Surface Mounted (NSM) with Carbon Fibre Reinforced Polymer (CFRP) laminates is a strengthening technique of high potential to increase the shear resistance of Reinforced Concrete (RC) beams that have some risk of collapsing in a brittle shear failure mode. This technique is based on introducing CFRP laminates into slits opened on the concrete cover of the lateral faces of the beam and bonded to concrete by an epoxy adhesive [1]. The efficiency of the NSM technique with CFRP laminates for the shear strengthening of RC beams has already been assessed by experimental research [1-3]. Dias and Barros [1] concluded that NSM technique is more effective than Externally Bonded Reinforcement (EBR) technique, since NSM provided a larger increase not only in terms of maximum load, but also in terms of load carrying capacity after shear crack formation. The NSM also provided higher values of the maximum strains measured in the CFRP (better utilization of the tensile strength of the CFRP material).

Available research shows that the predictive performance of computer programs based on the finite element method (FEM) and incorporating constitutive models for the material nonlinear analysis of RC structures failing in shear is quite dependent on the constitutive model adopted to simulate the shear stress transfer in the cracked concrete [4, 5]. In fact, Suryanto *et al.* [5] have evidenced that, for capturing correctly the deformational behaviour and the crack pattern of RC elements failing in shear by using a smeared crack approach, it is fundamental the adoption of a shear stress-shear strain softening law for modelling the damage that occurs during sliding/opening process of a cracked cement based material. Recently a total crack shear stress-shear strain approach was implemented in a multi-directional fixed smeared crack model for a better simulation of the strengthened beams failing in shear and in flexural/shear [6]. This approach was able of simulating the decrease of the total crack shear stress with the crack opening, but the stiffness predicted by the model for the behaviour of some beams was higher than the one registered experimentally. Furthermore, due to numerical instabilities some simulations were not capable of attaining the deflection corresponding to the peak load.

In this paper a softening diagram is proposed for modelling the sliding component of the crack constitutive law, and it was implemented into a multi-directional fixed smeared crack model for capturing with high

accuracy, not only the deformational and load carrying capacity of RC beams failing in shear, but also the crack patterns formed during the loading process of this type of structural elements.

To appraise the predictive performance of this model, it was applied on the simulation of an experimental program composed a series of T cross section RC beams with a certain percentage of steel stirrups and shear strengthened according to the NSM technique with CFRP laminates that is described in detail elsewhere [1]. For this purpose it was simulated nine beams with distinct NSM CFRP shear strengthening configurations: three inclinations of the laminates (45º, 60º and 90º); three percentages of CFRP. This experimental program was used to demonstrate the shear strengthening effectiveness of the NSM technique for RC beams. The constitutive model is briefly described in this paper, with the main focus on the innovative aspects implemented in an already existing multi-directional fixed smeared crack model [7].The predictive performance of the proposed model is assessed by simulating the experimental tests.

2. NUMERICAL MODEL

2.1. Introduction

In the present work is described a multi-directional fixed smeared crack model capable of simulating with high accuracy RC beams failing in shear. The main innovative aspect in this constitutive model is the treatment of the concrete fracture mode II by using a softening diagram to simulate the crack shear stress vs crack shear sliding in the context of a smeared approach. The executed parametric study reveals the relevance of this enhancement on the constitutive model in order to be possible to capture the deformational response and the crack pattern of RC beams failing in shear.

2.2. Multi-directional fixed smeared crack model

Under the framework of the finite element analysis, the tested beams are considered as a plane stress problem. The description of the formulation of the multi-directional fixed smeared crack model is restricted to the case of cracked concrete, at the domain of an integration point (*IP*) of a plane stress finite element. According to the adopted constitutive law, stress and strain are related by the following equation

$$\Delta\underline{\sigma} = \underline{D}^{crco}\ \Delta\underline{\varepsilon} \tag{1}$$

being $\Delta\underline{\sigma} = \{\Delta\sigma_1, \Delta\sigma_2, \Delta\tau_{12}\}^T$ and $\Delta\underline{\varepsilon} = \{\Delta\varepsilon_1, \Delta\varepsilon_2, \Delta\gamma_{12}\}^T$ the vectors of the incremental stress and incremental strain components.

Due to the decomposition of the total strain into an elastic concrete part and a crack part, $\Delta\underline{\varepsilon} = \Delta\underline{\varepsilon}^{co} + \Delta\underline{\varepsilon}^{cr}$, in equation (1) the cracked concrete constitutive matrix, $\underline{D}^{crco}$, is obtained with the following equation [6]:

$$\underline{D}^{crco} = \underline{D}^{co} - \underline{D}^{co}\left[\underline{T}^{cr}\right]^{T}\left(\underline{D}^{cr} + \underline{T}^{cr}\,\underline{D}^{co}\left[\underline{T}^{cr}\right]^{T}\right)^{-1}\underline{T}^{cr}\,\underline{D}^{co} \tag{2}$$

where $\underline{D}^{co}$ is the constitutive matrix of concrete, assuming a linear behaviour

$$\underline{D}^{co} = \frac{E_c}{1-\nu_c^2}\begin{bmatrix} 1 & \nu_c & 0 \\ \nu_c & 1 & 0 \\ 0 & 0 & \frac{1-\nu_c}{2} \end{bmatrix} \tag{3}$$

being E_c and ν_c the Young's modulus and the Poisson's ratio of concrete, respectively. In equation (2) $\underline{T}^{cr}$ is the matrix that transforms the stress components from the coordinate system of the finite element to the local crack coordinate system (a subscript ℓ is used to identify entities in the local crack coordinate system). If *m* cracks occurs at an *IP*

$$\underline{T}^{cr} = \left[\underline{T}_1^{cr} \quad \ldots \quad \underline{T}_i^{cr} \quad \ldots \quad \underline{T}_m^{cr}\right]^{T} \tag{4}$$

where the matrix crack orientation of a generic i^{th} crack is defined by

$$\underline{T}_i^{cr} = \begin{bmatrix} \cos^2\theta_i & \sin^2\theta_i & 2\sin\theta_i\cos\theta_i \\ -\sin\theta_i\cos\theta_i & \sin\theta_i\cos\theta_i & \cos^2\theta_i - \sin^2\theta_i \end{bmatrix} \tag{5}$$

with θ_i being the angle between the x_1 axis and the vector orthogonal to the plane of the i^{th} crack.

In equation (2) $\underline{D}^{cr}$ is a matrix that includes the constitutive law of the *m* cracks

$$\underline{D}^{cr} = \begin{bmatrix} \underline{D}_1^{cr} & \ldots & \underline{0} & \ldots & \underline{0} \\ \ldots & \ldots & \ldots & \ldots & \ldots \\ \underline{0} & \ldots & \underline{D}_i^{cr} & \ldots & \underline{0} \\ \ldots & \ldots & \ldots & \ldots & \ldots \\ \underline{0} & \ldots & \underline{0} & \ldots & \underline{D}_m^{cr} \end{bmatrix} \tag{6}$$

with $\underline{D}_i^{cr}$ being the crack constitutive matrix of the i^{th} crack

$$\underline{D}_i^{cr} = \begin{bmatrix} D_{I,i}^{cr} & 0 \\ 0 & D_{II,i}^{cr} \end{bmatrix} \tag{7}$$

where $D_{I,i}^{cr}$ and $D_{II,i}^{cr}$ represent, respectively, the modulus correspondent to the fracture mode I (normal) and fracture mode II (shear) of the i^{th} crack.

The behaviour of non-completely closed cracks formed in an *IP* is governed by the following relationship

$$\Delta\underline{\sigma}_{\ell}^{cr} = \underline{D}^{cr}\Delta\underline{\varepsilon}_{\ell}^{cr} \tag{8}$$

where $\Delta\underline{\sigma}_{\ell}^{cr}$ is the vector of the incremental crack stress components in the coordinate system of each of the *m* cracks

$$\Delta\underline{\sigma}_{\ell}^{cr} = \left[\Delta\sigma_{n,1}^{cr} \quad \Delta\tau_{nt,1}^{cr} \quad ... \quad \Delta\sigma_{n,i}^{cr} \quad \Delta\tau_{nt,i}^{cr} \quad ... \quad \Delta\sigma_{n,m}^{cr} \quad \Delta\tau_{nt,m}^{cr}\right]^{T} \tag{9}$$

and $\Delta\underline{\varepsilon}_{\ell}^{cr}$ is the vector of the correspondent incremental crack strain components

$$\Delta\underline{\varepsilon}_{\ell}^{cr} = \left[\Delta\varepsilon_{n,1}^{cr} \quad \Delta\gamma_{nt,1}^{cr} \quad ... \quad \Delta\varepsilon_{n,i}^{cr} \quad \Delta\gamma_{nt,i}^{cr} \quad ... \quad \Delta\varepsilon_{n,m}^{cr} \quad \Delta\gamma_{nt,m}^{cr}\right]^{T} \tag{10}$$

By using the $\underline{T}^{cr}$ matrix, the vector of the incremental crack strain components in the finite element coordinate system, $\Delta\underline{\varepsilon}^{cr}$, can be obtained from $\Delta\underline{\varepsilon}_{\ell}^{cr}$

$$\Delta\underline{\varepsilon}^{cr} = \left[\underline{T}^{cr}\right]^{T}\Delta\underline{\varepsilon}_{\ell}^{cr} \tag{11}$$

and the equilibrium condition

$$\Delta\underline{\sigma}_{\ell}^{cr} = \underline{T}^{cr}\Delta\underline{\sigma} \tag{12}$$

must be assured.

In the present approach, a new crack is arisen in an *IP* when the angle formed between the new crack and the already existing cracks, θ_{new}^{cr}, exceeds a certain threshold angle, θ_{th} (a parameter of the constitutive model that in general ranges between 30 and 60 degrees [7]).

The crack opening propagation is simulated with the trilinear diagram represented in Figure 1, which is defined by the normalized stress, α_i, and strain, ξ_i, parameters that define the transition points between the linear segments of this diagram. The ultimate crack strain, $\varepsilon_{n,u}^{cr}$, is defined as a function of the parameters α_i and ξ_i, fracture energy, G_f^I, tensile strength, $f_{ct} = \sigma_{n,1}^{cr}$, and crack band width, l_b, as follows [7],

$$\varepsilon_{n,u}^{cr} = \frac{2}{\xi_1 + \alpha_1\xi_2 - \alpha_2\xi_1 + \alpha_2}\frac{G_f^I}{f_{ct}l_b} \tag{13}$$

being $\alpha_1 = \sigma_{n,2}^{cr}/\sigma_{n,1}^{cr}$, $\alpha_2 = \sigma_{n,3}^{cr}/\sigma_{n,1}^{cr}$, $\xi_1 = \varepsilon_{n,2}^{cr}/\varepsilon_{n,u}^{cr}$ and $\xi_2 = \varepsilon_{n,3}^{cr}/\varepsilon_{n,u}^{cr}$.

To simulate the fracture mode II modulus, D_{II}^{cr}, a shear retention factor is currently used [7, 8]:

$$D_{II}^{cr} = \frac{\beta}{1-\beta}G_c \tag{14}$$

where G_c is the concrete elastic shear modulus and β is the shear retention factor. The parameter β is defined as a constant value or as a function of the current crack normal strain, ε_n^{cr}, and of the ultimate crack normal strain, $\varepsilon_{n,u}^{cr}$, as follows,

$$\beta = \left(1 - \frac{\varepsilon_n^{cr}}{\varepsilon_{n,u}^{cr}}\right)^{p_1} \tag{15}$$

When $p_1 = 1$ a linear decrease of β with the increase of ε_n^{cr} is assumed. Larger values of the exponent p_1 correspond to a more pronounced decrease of the β parameter [7].

In structures governed by flexural failure modes, this strategy leads to simulations with reasonable accuracy. Exceptions occur in structures that fail by the formation of a critical shear crack. To simulate accurately the deformational response and the crack pattern up to the failure of this type of structures, the adoption of a softening crack shear stress *vs.* crack shear strain relationship is the strategy explored in the present work. In fact, Suryanto *et al.* have already demonstrated that the adoption of a shear softening law for modelling the shear stress transfer in cracked concrete is fundamental for a proper simulation of the behaviour of engineered cement composites (ECC) beams failing in shear [5]. The law proposed by these authors for simulating the crack shear stress-shear sliding response of ECC is based on the model developed by Li *et al.* [9]. This law was implemented by Suryanto *et al.* in a fixed smeared crack model where two orthogonal cracks can be formed in an integration point of a finite element. However, experimental evidence of RC structures failing in shear shows that in the critical shear regions non-orthogonal cracks are formed [1-3, 11, 12], thereby in the present work a softening law for modelling the fracture mode II of cement based materials was implemented in the above described multi-directional fixed smeared crack model, where several cracks can be formed in the same integration point based on a stress criterion and a threshold angle between cracks.

The implemented crack shear diagrams are represented in Figure 2, but the presentation of the formulation will be focused on the linear diagram (Figure 2a), being the formulations for the other diagrams available elsewhere [10]. The crack shear stress increases linearly until the crack shear strength is reached, $\tau_{t,p}^{cr}$, (first branch of the shear crack diagram), followed by a decrease in the shear residual strength (softening branch). The diagram represented in Figure 2a is defined by the following equations:

$$\tau_t^{cr}\left(\gamma_t^{cr}\right)=\begin{cases} D_{t,1}\,\gamma_t^{cr} & 0<\gamma_t^{cr}\le\gamma_{t,p}^{cr} \\ \tau_{t,p}^{cr}-\dfrac{\tau_{t,p}^{cr}}{\left(\gamma_{t,u}^{cr}-\gamma_{t,p}^{cr}\right)}\left(\gamma_t^{cr}-\gamma_{t,p}^{cr}\right) & \gamma_{t,p}^{cr}<\gamma_t^{cr}\le\gamma_{t,u}^{cr} \\ 0 & \gamma_t^{cr}>\gamma_{t,u}^{cr} \end{cases} \tag{16}$$

The initial shear fracture modulus, $D_{t,1}^{cr}$, is defined by equation (14) (D_{II}^{cr} is replaced by $D_{t,1}^{cr}$) by assuming for β a constant value in the range]0,1[. The peak crack shear strain, $\gamma_{t,p}^{cr}$, is obtained using the crack shear strength (from the input data), $\tau_{t,p}^{cr}$, and the crack shear modulus:

$$\gamma_{t,p}^{cr}=\frac{\tau_{t,p}^{cr}}{D_{t,1}^{cr}} \tag{17}$$

The ultimate crack shear strain, $\gamma_{t,u}^{cr}$, depends on the crack shear strength, $\tau_{t,p}^{cr}$, on the shear fracture energy (mode II fracture energy), $G_{f,s}$, and on the crack bandwidth, l_b:

$$\gamma_{t,u}^{cr}=\frac{2G_{f,s}}{\tau_{t,p}^{cr}\,l_b} \tag{18}$$

In the present approach it is assumed that the crack bandwidth, used to assure that the results are independent of the mesh refinement [8], is the same for both fracture mode I and mode II processes, but specific research should be done in this respect in order to assess the influence of these model parameters on the predictive performance of the behaviour of elements failing in shear.

When the softening constitutive law represented in Figure 2 is used to evaluate the fracture mode II softening modulus D_{II}^{cr} of equation (7), its value depends on the branches defining the diagram. For this reason five shear crack statuses are proposed and their meaning is schematically represented in Figure 2a. The crack mode II modulus of the first linear branch of the diagram is defined by equation (14), the second linear softening branch is defined by

$$D_{II}^{cr}=D_{t,2}^{cr}=-\frac{\tau_{t,p}^{cr}}{\gamma_{t,u}^{cr}-\gamma_{t,p}^{cr}} \tag{19}$$

and the crack shear modulus of the unloading and reloading branches is obtained from

$$D_{II}^{cr}=D_{t,3-4}^{cr}=\frac{\tau_{t,\max}^{cr}}{\gamma_{t,\max}^{cr}} \tag{20}$$

being $\gamma_{t,\max}^{cr}$ and $\tau_{t,\max}^{cr}$ the maximum crack shear strain already attained and the corresponding crack shear stress determined from the softening linear branch. Both components are stored to define the unloading/reloading branch (see Figure 2a).

In free-sliding status ($\left|\gamma_t^{cr}\right| > \left|\gamma_{t,u}^{cr}\right|$) the crack mode II stiffness modulus, $D_{II}^{cr} = D_{t,5}^{cr}$, is null. To avoid numerical instabilities in the calculation of the stiffness matrix and in the calculation of the internal forces, when the crack shear status is free-sliding, a residual value is assigned to this term.

A free-sliding status is assigned to the shear crack status when $\varepsilon_n^{cr} > \varepsilon_{n,u}^{cr}$. The details about how the shear crack statuses were treated can be consulted elsewhere [10].

3. PREDICTIVE PERFORMANCE OF THE NUMERICAL MODEL

3.1 Introduction

To assess the predictive performance of the model described in previous section, the experimental tests carried out with a series of T cross section RC beams shear strengthened according to the NSM technique by using CFRP laminates were simulated. The experimental program corresponding to tests of these beams is described in detail elsewhere [1], so only a brief resume of this program is given in the following sections.

3.2 Series of beams

Figure 3 presents the T cross section of the ten beams comprising the experimental program. The reinforcement systems were designed to assure shear failure mode for all the tested beams. To localize shear failure in only one of the beam shear spans, a three point load configuration of a distinct length of the beam shear spans was selected, as shown in Figure 3. The monitored beam span (L_i) is 2.5 times the effective depth of the beam ($L_i/d=2.5$). To avoid shear failure in the L_r beam span, steel stirrups ϕ6@75mm were applied in this span. The differences between the tested beams are restricted to the shear reinforcement systems applied in the L_i beam span. The experimental program is made up of one beam with steel stirrups ϕ6@300mm (2S-R beam, with a percentage of stirrups, ρ_{sw}, of 0.10%); and nine beams of ϕ6@300mm that include distinct CFRP arrangements on the L_i beam span (three distinct percentages of CFRP laminates and, for each CFRP percentage, three inclinations for the laminates, 90º, 60º and 45º, Figure 4). The CFRP shear strengthening percentage, ρ_{fw}, was obtained from:

$$\rho_{fw} = \frac{2 \cdot a_f \cdot b_f}{b_w \cdot s_f \cdot \sin\theta_f} \tag{21}$$

where a_f = 1.4 mm and b_f = 9.5 mm are the dimensions of the laminate cross section. In equation (21), b_w = 180 mm is the beam web width, and s_f and θ_f represent the spacing and inclination of the CFRP,

respectively. The strengthening technique is composed of the following procedures: 1) using a diamond cutter, slits of about 5 mm width and 12-15 mm depth were opened on the concrete cover (of about 22 mm thickness) of the lateral faces of the beam web (Figure 3.2), according to the pre-defined arrangement for the laminates (the laminates were not anchored to the beam flange, they were restricted to the beam web, Figure 4); 2) the slits were cleaned by compressed air; 3) the laminates were cleaned with acetone; 4) the epoxy adhesive was produced according to supplier recommendations; 5) the slits were filled with the adhesive; 6) the adhesive was applied on the faces of the laminates; and 7) the laminates were inserted into the slits and adhesive in excess was removed. To guarantee a proper curing of the adhesive, at least one week passed between the beam strengthening operations and the beam test.

3.3 Test setup and monitoring system

The three point beam bending tests were carried out using a servo closed-loop control equipment, taking the signal in the displacement transducer (LVDT) positioned at the loaded section, to control the test at a deflection rate of 0.01 mm/s. To avoid concrete spalling at the most loaded beam support, a confinement system based on the use of wet lay-up CFRP sheets was applied (three layers with the fibres direction coinciding with the beam axis direction).

Four strain gauges (SG_L) were bonded in each of the monitored CFRP laminates (two per beam) according to the arrangement represented in Figure 5a, and one steel stirrup positioned in the L_i shear span was monitored with three strain gauges (SG_S) installed according to the configuration represented in Figure 5b. The location of the monitored laminates and stirrups in the tested beams is represented in Figure 4.

3.4 Main results

The relationships between the applied force and the deflection at the loaded section for the tested beams are presented in Figure 6.

The results show that, for deflection higher than the one corresponding to the formation of the first shear crack in the 2S-R reference beam, the adopted CFRP laminates configurations provided a significant increase in the beam's load carrying capacity. In fact, the decrease of stiffness observed in the 2S-R reference beam when the first shear crack was formed was not so significant in the CFRP shear strengthened beams. This reveals that the CFRP laminates bridging the surfaces of the shear crack offer resistance, mainly, to crack opening, resulting a smaller degradation of the shear stress transfer between the faces of

the crack due to aggregate interlock effect. Therefore, for deflections above the deflection corresponding to the formation of the shear crack in the 2S-R reference beam, an increase of the beam's stiffness is observed in the shear strengthened beams. The crack opening resisting mechanisms provided by the laminates bridging the cracks also contribute to increase the load at which yield initiation occurs in the stirrups.

The strengthening arrangements with the lowest ρ_{fw} had the smallest increase in terms of the beam load carrying capacity (11.1%, 29.3% and 27.2% for the beams strengthened with vertical laminates, and laminates at 45º and 60º, respectively). For the beams shear strengthened with the intermediate ρ_{fw}, the strengthening configurations of vertical laminates, and laminates at 45º and 60º assured an increase in the beam load carrying capacity of 23.1%, 38.8%, and 29.8%, respectively. Among the beams strengthened with the highest ρ_{fw}, as already happened for the other two percentages, the strengthening configuration of θ_f = 45º was the most effective in terms of maximum load capacity, since an increase of 47.0% (2S-10LI45) was obtained, while an increase of 30.8% (2S-10LV) and 35.8% (2S-9LI60) was recorded for the strengthening arrangements of θ_f =90º and θ_f =60º, respectively. Regardless of the percentage of CFRP it was verified that inclined laminates are more effective than vertical laminates. Furthermore, an increase of the percentage of CFRP led to an increase of the beam's shear resistance. A very important aspect of the effectiveness of the NSM technique, regarding the analysed beams, is its capacity to mobilize the yield strain of the stirrups crossed the diagonal shear failure crack at the maximum load of the strengthened beams.

The global analysis of the failure modes of the tested beams with CFRP laminates indicates that the efficacy of NSM technique for the shear strengthening of RC beams increases with the concrete strength [11, 12]. In fact the failure process includes fracture of the concrete surrounding the laminates, having the concrete become adhered to the detached laminates. In the beams with the highest percentage of CFRP the critical failure mode is governed by a group effect of the laminates that consists on the premature detachment of a concrete layer that includes the laminates.

3.5 Finite element mesh, integration schemes and constitutive laws for the materials

To simulate the crack initiation and the fracture mode I propagation of reinforced concrete, the trilinear tension-softening diagram represented in Figure 1 was adopted. The values that define this diagram are indicated in Table 1, and were obtained from the experimental program for the characterization of the

relevant properties of the intervening materials. In this table is also included the data necessary to define the shear-softening diagram represented in Figure 2a, adopted to simulate the degradation of crack shear stress transfer after crack initiation. Since no available experimental results exist to characterize the crack shear softening diagram, the adopted values were obtained by inverse analysis by fitting the experimental results as best as possible.

In Figure 7 is represented, as an example, the finite element mesh used for the simulation of the 2S-4LI45 beam. The beams are modelled with a mesh of 4-noded serendipity plane stress finite elements. The longitudinal steel bars, stirrups and the NSM CFRP laminates are modelled with 2-noded perfect bonded embedded cables (one degree-of-freedom per each node).

For modelling the behaviour of the longitudinal and transversal steel bars, the stress-strain relationship represented in Figure 8 was adopted. The curve (under compressive or tensile loading) is defined by the points PT1=$(\varepsilon_{sy}, \sigma_{sy})$, PT2=$(\varepsilon_{sh}, \sigma_{sh})$ and PT3=$(\varepsilon_{su}, \sigma_{su})$, and a parameter p that defines the shape of the last branch of the curve. Unloading and reloading linear branches with slope $E_s = \sigma_{sy} / \varepsilon_{sy}$ are assumed in the present approach. The values of the parameters of the constitutive model for the steel are indicated in Table 2.

For modelling the NSM CFRP laminates, a linear elastic stress-strain relationship was adopted. Table 3 present the values obtained in experimental tests with CFRP laminates specimens.

3.6 Simulations and discussion

The experimental and the numerical relationships between the applied load and the deflection at the loaded section for the tested beams are compared in Figure 9. The crack patterns of these beams at the end of the analysis (at the end of the last converged load increment) are compared with the obtained experimental crack patterns in Figure 10. These two figures show that the numerical model is able to capture with good accuracy the deformational response of the beams and captured with good precision the localization and profile of the shear failure crack.

Figure 11 also shows that the numerical simulations fit with good accuracy the strains measured in the steel stirrups and NSM laminates, which means that the assumption of perfect bond between steel stirrups and NSM laminates and surrounding concrete is acceptable, at least in the design point of view for the serviceability and ultimate limit states. The results correspond to 2S-4LI45, but similar level of accuracy was obtained in the simulations of the other beams.

3.7 Simulation of experimental tests carried out by other authors with NSM strengthened RC beams failed in shear

To have a better assessment of the predictive performance of the developed model, it was used on the simulation of the experimental tests carried out by Chaallal *et al.* [13] with a series of RC beams shear strengthened with NSM FRP reinforcements. Figure 12 represents the geometry of the numerically simulated full scale T-beams. For the numerical simulations it was selected two series of two beams each (Table 4), the S0 series without steel stirrups, and the S1 series with steel stirrups of 8 mm diameter at a spacing of 175 mm. The S0-CON control beam has no type of shear reinforcement, while the S0-NSM beam is shear strengthened with vertical CFRP rods spaced at 130 mm, placed in the span length 1050 mm of the beam where the shear failure is expected to occur (Figure 12d). In the S1 series, the S1-CON beam is shear reinforced with steel stirrups, while S1-NSM beam also includes vertical CFRP rods spaced at 130 mm. The longitudinal reinforcement consists of four bars of 25 mm diameter disposed in two layers in the tensile zone, and six bars of 10 mm diameter in the compression zone (Figure 12c).

The concrete beams are modelled with a mesh of 4-noded serendipity plane stress finite elements. The concrete properties in the numerical simulations are included in Table 5, and, apart the crack shear softening diagram, they were obtained from the information available in the reference [13]. For the crack shear softening diagram, values similar to those adopted in the simulations described in Section 3.5 were adopted, with minor adjustments, taking into account the differences on the intervening materials in these two test programs.

The longitudinal steel bars, stirrups and the NSM CFRP rods are modelled with 2-noded perfect bonded embedded cables (one degree-of-freedom per each node). The behaviour of the longitudinal and transversal steel bars is simulated by the stress-strain relationship represented in Figure 8, whose values of the variables that define this diagram are included in Table 6. The tensile strength, the modulus of elasticity and the ultimate tensile strain of the CFRP rods of 9.5 mm diameter was, respectively, 1885 MPa, 148 GPa and 1.26% [13].

Figure 13 compares the relationship between the applied load and the deflection at the loaded section recorded experimentally and obtained in the numerical simulations. These results confirm the capability of the developed model to simulate the behaviour of RC beams failing in shear.

3.7 Influence of the parameters that define the crack shear softening diagram

To assess the influence of the parameters that define the crack shear softening diagram (Figure 2a) on the load-deflection relationship predicted by the numerical model, the values of these parameters are modified from those used in the previous section. For this study the 2S-4LI45 beam was selected, but the conclusions to be extracted have a generalized character.

3.7.1 Influence of $G_{f,s}$

Figure 14 compares the load versus deflection at loaded section obtained for three different values of the shear fracture energy ($G_{f,s}$), 0.01, 0.05 and 1.0 N/mm (all the remaining parameters were maintained the same), the first one is lower and the last one is higher than the value considered in the analysis of the section 3.6 (0.05 N/mm). This figure also compares the crack patterns obtained in the simulations corresponding to these three values of $G_{f,s}$. As expected, by increasing $G_{f,s}$ the stiffness and the load carrying capacity also increase. The crack patterns revealed that by increasing $G_{f,s}$ more shear cracks are formed due to the higher crack shear stress transfer.

3.7.2 Influence of $\tau_{t,p}^{cr}$

Figure 15 compares the load versus deflection at loaded section obtained for three different values of the crack shear strength ($\tau_{t,p}^{cr}$), 0.5, 1.1 and 4.0 MPa (all the remaining parameters were maintained the same), the first one is lower and the last one is higher than the value considered in the analysis of the section 3.6 (1.1 MPa). As expected, the stiffness and the load carrying capacity after the formation of the critical shear failure crack of the simulation with the larger $\tau_{t,p}^{cr}$ were much higher than in the other two cases. The responses for the $\tau_{t,p}^{cr}$ of 0.5 and 1.1 MPa were similar, but a close inspection on these responses reveals that the one corresponding to $\tau_{t,p}^{cr}$ =1.1 MPa was stiffer in the initial part and less stiff in the final part, which is justified by the crack shear stress-crack shear strain diagrams represented in Figure 16. In fact, in the simulation with a higher crack shear strength ($\tau_{t,p}^{cr}$ =1.1 MPa) the cracks have entered in the softening phase at larger deflection of the beam, but due to the constant value adopted for the $G_{f,s}$, the softening response for this diagram was more brittle, conducting to a higher decrease of the beam's stiffness. At ultimate deflection, the crack pattern corresponding to the smaller $\tau_{t,p}^{cr}$ (0.5 MPa) includes a well-defined shear

failure crack (completely open), while the crack pattern representative of the larger $\tau_{t,p}^{cr}$ (4.0 MPa), does not include any crack completely open.

3.7.3 Influence of β parameter defining the first branch of the $\tau_t^{cr} - \gamma_t^{cr}$ diagram

To evaluate peak crack shear strain, $\gamma_{t,p}^{cr}$, (Eq. (17)) it is necessary to determine the initial shear fracture modulus, $D_{t,1}^{cr}$, which defined by Eq. (14) by attributing a certain value to the shear retention factor, β. To assess the influence of this parameter on the response of the beam in analysis, three values were considered, 0.05, 0.4 and 0.8, the first one is lower and the last one is higher than the value considered in the analysis of the section 3.6 (0.4). Figure 17 shows that this parameter has an influence similar to $\tau_{t,p}^{cr}$, since as larger is β as stiffer is the initial branch of the first branch of the $\tau_t^{cr} - \gamma_t^{cr}$ diagram and softer is the softening branch of this diagram (Figure 16). In fact, up to a deflection of about 2mm (that corresponds to the formation of the shear failure crack in the reference beam), the load carrying capacity of the beam increases with β, but for larger deflections, when the influence of softening branch of the $\tau_t^{cr} - \gamma_t^{cr}$ diagram becomes relevant, the load carrying capacity of the beam increases with the decrease of β, due to the higher crack shear stress transfer (Figure 18).

3.7.4 Shear retention factor versus softening diagram for modelling the crack shear behaviour

Figure 19 compares the relationship between the force and the deflection at loaded section for the beam in analysis when using the concept of shear retention factor, β, (Eq. (15) with p_1=3) and adopting the $\tau_t^{cr} - \gamma_t^{cr}$ diagram already used in the simulations of section 3.6. Up to a deflection of about 2mm (that corresponds to the formation of the shear failure crack in the reference beam) the responses are similar, but above this deflection limit the two approaches start diverging significantly. The β approach has predicted a much higher load carrying capacity than the correct one predicted when using the $\tau_t^{cr} - \gamma_t^{cr}$ diagram. Since the β approach implemented in an incremental model, like the one described in the present work, is not capable of simulating a decrease of the crack shear stress transfer (τ_t^{cr}) with the increase of the crack shear strain (γ_t^{cr}), this approach has incorrectly predicted a flexural failure mode.

4. CONCLUSIONS

This study presents the relevant results of an experimental program for the assessment of the effectiveness of the NSM technique with CFRP laminates for the shear strengthening of RC beams with a certain percentage of steel stirrups. From the obtained results, it can be concluded that:

- The NSM laminates provided a large increase in terms of load carrying capacity after shear crack formation compared to reference beam.
- The effectiveness level of the NSM technique was limited by the concrete tensile strength, since at failure, a certain concrete volume was attached to the laminates. The failure modes of the beam with NSM laminates were also influenced by the percentage of the CFRP laminates.
- Inclined laminates were more effective than vertical laminates and an increase of the percentage of laminates led to an increase of the shear capacity of the beams.

The capability of a FEM-based computer program to predict with high accuracy the behaviour of this type of structures up to its collapse was highlighted. The introduction of the shear crack softening diagram into the multi-directional fixed smeared crack model allowed a good prediction of the deformational behaviour, load carrying capacity, crack pattern and strain fields in the reinforcements of the tested beams Due to the lack of specific experimental tests, the data to define the shear crack softening diagram was obtained by inverse analysis. It can be concluded that the implementation of the shear softening diagram in the multi-directional fixed smeared crack model available in the FEMIX computer program has improved its capabilities to predict with higher accuracy the behaviour of structures failing in shear or in flexural/shear. A parametric study was carried out to assess the influence of the parameters that define the crack shear softening diagram ($\tau_t^{cr} - \gamma_t^{cr}$) on the structural response of the type of beams analysed in the present work. It was verified that the load carrying capacity of the beams increase with $G_{f,s}$, while increasing $\tau_{t,p}^{cr}$ or β (both parameters used to define the $\tau_t^{cr} - \gamma_t^{cr}$ diagram) has similar tendency by increasing the load carrying capacity of the beam up to a certain deflection of the beam (when shear governing cracks are formed), followed by a decrease due to a more brittle behaviour of the softening branch of the $\tau_t^{cr} - \gamma_t^{cr}$ diagram. Finally, by using the concept of shear retention factor, β , for modelling the crack shear stress transfer, an abnormal high load carrying capacity is estimated, with an incorrectly predicted flexural failure mode, while adopting a $\tau_t^{cr} - \gamma_t^{cr}$ softening diagram, not only the response of the beam, but also the failure mode and the crack pattern are correctly estimated.

5. ACKNOWLEDGEMENTS

The authors wish to acknowledge the support provided by the "Empreiteiros Casais", Degussa, S&P®, and Secil (Unibetão, Braga) companies. The study reported in this paper is part of the research project PTDC/ECM/114511/2009, supported by the Portuguese Foundation for Science and Technology (FCT).

REFERENCES

[1] Dias, S.J.E. and Barros J.A.O., 2010. Performance of reinforced concrete T beams strengthened in shear with NSM CFRP laminates. Engineering Structures, 32(2), 373-384.

[2] Kotynia, R., 2007. Shear strengthening of RC beams without NSM CFRP laminates. 8th International Symposium on Fiber Reinforced Polymer Reinforcement for Concrete Structures (FRPRCS-8), Patras, Greece.

[3] El-Hacha, R. and Wagner, M., 2009. Shear Strengthening of Reinforced Concrete Beams using Near-Surface Mounted CFRP Strips. 9th International Symposium on Fiber Reinforced Polymers Reinforcement for Concrete Structures (FRPRCS-9), Sydney, Australia, July, 10 pp.

[4] Rots, J.G. and de Borst, R., 1987. Analysis of mixed-mode fracture in concrete. Journal of Engineering Mechanics–ASCE, 113(11): 1739-1758.

[5] Suryanto, B.; Nagai, K.; Maekawa, K., "Modeling and analysis of shear-critical ECC members with anisotropic stress and strain fields", Journal of Advanced Concrete Technology, 8(2), 239-258, June 2010.

[6] Barros, J.A.O., Costa, I. G. and Ventura-Gouveia, A., 2011. CFRP flexural and shear strengthening technique for RC beams: experimental and numerical research. Advances in Structural Engineering Journal, 14(3), 559-581.

[7] Sena-Cruz, J.M., 2004. Strengthening of concrete structures with near-surface mounted CFRP laminate strips. PhD Thesis, Department of Civil Engineering, University of Minho. http://www.civil.uminho.pt/composites.

[8] Rots, J.G., 1988. Computational modeling of concrete fracture. PhD Thesis, Delft University of Technology.

[9] Li, B., Maekawa, K. and Okamura, H., 1989. Contact density model for stress transfer across cracks in concrete. Journal of the faculty of engineering, the University of Tokyo (B), 40(1), 9-52.

[10] Ventura-Gouveia, A., 2011. Constitutive models for the material nonlinear analysis of concrete structures including time dependent effects. PhD Thesis, Department of Civil Engineering, University of Minho.

[11] Dias, S.J.E.; Barros, J.A.O., 2011. Shear strengthening of RC T-section beams with low concrete using NSM CFRP laminates. Journal Cement & Concrete Composites, 33(2), 334-345.

[12] Dias, S.J.E.; Barros, J.A.O., 2012. NSM shear strengthening technique with CFRP laminates applied in high-strength concrete beams with or without pre-cracking. Composites Part B: Engineering Journal, 43(2), 290-301.

[13] Chaallal, O., Mofidi, A., Benmokrane, B., Neale, K., 2011. Embedded through-section FRP rod method for shear strengthening of RC beams: performance and comparison with existing techniques. Composites for Construction, 15(3), 374-383.

NOTATION

a_f = CFRP width

b_f = CFRP thickness

b_w = beam web width

CFRP = carbon fibre reinforced polymer

d = effective depth of the longitudinal steel bars

D_{Ii}^{cr} = opening fracture mode stiffness modulus of the i^{th} branch of the stress-strain diagram to simulate the fracture mode I crack propagation

$D_{I,i}^{cr}$ = crack constitutive matrix component relative to the i^{th} crack normal opening mode (mode I)

$D_{I,k}^{cr}$ = crack constitutive matrix component relative to the crack normal opening mode (mode I) for the k iteration

$D_{II,i}^{cr}$ = crack constitutive matrix component relative to the i^{th} crack sliding mode (mode II)

$D_{II,k}^{cr}$ = crack constitutive matrix component relative to the crack sliding mode (mode II) for the k iteration

$\underline{D}^{co}$ = elastic constitutive matrix

$\underline{D}^{cr}$ = crack constitutive matrix

$\underline{D}^{crco}$ = constitutive matrix for the cracked concrete

$\underline{D}^{cr}$ = constitutive matrix that takes into account the assembly of several (m) cracks with distinct directions

$\underline{D}_i^{cr}$ = crack constitutive matrix of the i^{th} crack

E_c = concrete elasticity modulus

E_f = modulus of elasticity of CFRP laminates and strips

E_s = Young's modulus of the longitudinal tensile steel bars

E_{sm} = modulus of elasticity of steel

f_{cm} = average compressive strength

f_{ct} = tensile strength

f_{fu} = tensile strength of the FRP

f_{sum} = steel tensile strength

f_{sym} = steel yield strength

F_{max} = maximum experimental load

F_{sy} = yield initiation load (at $\varepsilon_{sy,eq}$)

G_c = concrete elastic shear modulus

G_f^I = mode I fracture energy

IP = integration point

LVDT = linear voltage displacement transducer

l_b = crack band width

L_i = span length i

NSM = near surface mounted

$N_{cr,max}$ = Maximum number of cracks per each integration point

p = parameter that defines the shape of the last branch of the steel stress-strain curve

p_1 = shear degradation factor

p_2 = parameter defining the fracture energy available to the new crack

RC = reinforced concrete

s_f = distance between CFRP laminates

SG_L = strain-gauges installed on NSM laminates

SG_S = strain-gauges installed on longitudinal steel bars

t_f = thickness of FRP

$\underline{T}^{cr}$ = transformation matrix that takes into account the assembly of several (m) cracks with distinct directions

$\underline{T}_k^{cr}$ = transformation matrix that takes into account the assembly of several (m) cracks with distinct directions for the k iteration

$\underline{T}_i^{cr}$ = transformation matrix of the i^{th} crack

α_i = fracture parameters used to define the trilinear stress-strain softening diagram

β = shear retention factor

γ_{nt}^{cr} = crack shear strain

$\Delta\gamma_{nt,i}^{cr}$ = incremental crack shear strain of the i^{th} crack

$\Delta\varepsilon_{n,i}^{cr}$ = incremental crack normal strain of the i^{th} crack

$\Delta\underline{\varepsilon}$ = vector containing the strain incremental components

$\Delta\underline{\varepsilon}^{co}$ = vector containing the incremental strain of the uncracked concrete between the cracks

$\Delta\underline{\varepsilon}^{cr}$ = vector containing the incremental strain of the crack

$\Delta\underline{\varepsilon}_{\ell}^{cr}$ = vector of the incremental crack strain components in the crack coordinate system

$\Delta\sigma_{n,i}^{cr}$ = incremental crack normal stress of the i^{th} crack

$\Delta\underline{\sigma}$ = vector containing the stress incremental components

$\Delta\underline{\sigma}_{\ell}^{cr}$ = vector of the incremental crack stress components in the crack coordinate system

$\Delta\tau_{nt}^{cr}$ = incremental crack shear stress

$\Delta\tau_{nt,i}^{cr}$ = incremental crack shear stress of the i^{th} crack

ε_n^{cr} = crack normal strain

$\varepsilon_{n,i}^{cr}$ = crack normal strain used to define point i in the trilinear stress-strain softening diagram

$\varepsilon_{n,u}^{cr}$ = ultimate crack normal strain

ε_{sh} = strain corresponding to point 2 (PT2) of the steel stress-strain relationship

ε_{su} = strain corresponding to point 3 (PT3) of the steel stress-strain relationship

ε_{sy} = strain corresponding to point 1 (PT1) of the steel stress-strain relationship

θ_i = angle between the x_1 axis and the vector orthogonal to the plane of the i^{th} crack

θ_{new}^{cr} = orientation between the new crack and the already existing cracks

θ_{th} = threshold angle

θ_f = inclination of CFRP

ν_c = poisson's ratio

ξ_i = fracture parameters used to define the trilinear stress-strain softening diagram

ρ_f = strengthening ratio of the NSM laminates

$\rho_{l,eq}$ = equivalent flexural reinforcement ratio

ρ_{sl} = reinforcement ratio of the bottom longitudinal steel bars

σ_I = maximum principal tensile stress

σ_{k-1} = normal stress for the *k*-1 iteration

σ_n^{cr} = crack normal stress

$\sigma_{n,i}^{cr}$ = crack normal stress used to define point *i* in the trilinear stress-strain softening diagram

σ_{sh} = stress corresponding to point 2 (PT2) of the steel stress-strain relationship

σ_{su} = stress corresponding to point 3 (PT3) of the steel stress-strain relationship

σ_{sy} = stress corresponding to point 1 (PT1) of the steel stress-strain relationship

τ_{nt}^{cr} = crack shear stress

LIST OF TABLE CAPTIONS

Table 1: Values of the parameters of the concrete constitutive model.

Table 2: Values of the parameters of the steel constitutive model (see Figure 8).

Table 3: Properties of CFRP laminates.

Table 4: Details of the T-beams tested by Chaallal *et al.* [13].

Table 5: Concrete properties of the T-beams tested by Chaallal *et al.* [13].

Table 6: Properties of the steel reinforcements of the T-beams tested by Chaallal *et al.* [13].

Table 1: Values of the parameters of the concrete constitutive model.

Property	**Value**
Poisson's ratio (ν_c)	0.15
Initial Young's modulus (E_c)	33271 N/mm^2
Compressive strength (f_c)	39.7 N/mm^2
Trilinear tension-softening diagram	f_{ct} = 2.2 N/mm^2 ; G_f = 0.086 N/mm ξ_1 = 0.005; α_1 = 0.3; ξ_2 = 0.1; α_2 = 0.3
Parameter defining the mode I fracture energy available to the new crack [7]	$p_2 = 3$
Crack shear stress-crack shear strain softening diagram	$\tau_{t,p}^{cr}$ = 1.1 N/mm^2; $G_{f,s}$ =0.05 N/mm; β =0.4
Crack bandwidth, l_b	Square root of the area of Gauss integration point
Threshold angle [7]	α_{th} = 30º
Maximum number of cracks per integration point [7]	2

Table 2: Values of the parameters of the steel constitutive model (see Figure 8).

Property	**ϕ6**	**ϕ12**	**ϕ16**	**ϕ32**
$f_{sym}\,(N/mm^2)$	500	490	470	625
$f_{sum}\,(N/mm^2)$	594	591	566	905
$E_{sm}\,(N/mm^2)$	217	196	181	208
$\mathcal{E}_{sy}\,(‰)$	2.3	2.5	2.6	3
$\sigma_{sy}\,(N/mm^2)$	500	490	470	625
$\mathcal{E}_{sh}\,(‰)$	20	30	30	10
$\sigma_{sh}\,(N/mm^2)$	537	490	470	845
$\mathcal{E}_{su}\,(‰)$	45	215	220	50
$\sigma_{su}\,(N/mm^2)$	594	591	566	905
Third branch exponent	1	1	1	1

Table 3: Properties of CFRP laminates.

CFRP laminates	
Maximum tensile strength	f_{fum} = 2741.7 MPa
Young's Modulus	E_{fm} = 170.9 GPa
Maximum strain	ε_{fu} = 1.60%

Table 4: Details of the T-beams tested by Chaallal *et al.* [13].

Designation of the beams	Internal steel stirrups	Shear strengthening system	Spacing of CFRP rods (mm)
S0-CON	-	-	-
S0-NSM	-	Vertical CFRP rods	130
S1-CON	ϕ8 @ 175	-	-
S1-NSM	ϕ8 @ 175	Vertical CFRP rods	130

Table 5: Concrete properties of the T-beams tested by Chaallal *et al.* [13].

Property	**Value**
Poisson's ratio (ν_c)	0.15
Initial Young's Strength (E_c)	30000 N/mm^2
Compressive strength (f_c)	25 N/mm^2
Trilinear tension-softening diagram	f_{ct}=1.8 N/mm^2, , G_f=0.09 N/mm, ξ_1=0.004, α_1=0.25, ξ_2=0.1, α_2=0.15
Parameter defining the mode I fracture energy available to the new crack [7]	p_2=3
Crack shear stress-crack shear strain softening diagram	$\tau^{cr}_{t,p}$=1.2 N/mm^2, $G_{f,s}$=0.06 N/mm, β=0.5
Crack band width, l_b	Square root of the area of Gauss integration point
Threshold angle [7]	α_{th}=30˚
Maximum number of cracks per integration point [7]	2

Table 6: Properties of the steel reinforcements of the T-beams tested by Chaallal *et al.* [13].

Property	**ϕ*8* (M8)**	**ϕ*11.3* (M10)**	**ϕ*25.2* (M25)**
Area (mm^2)	50	100	500
f_{sym} (MPa)	540	470	470
f_{sum} (MPa)	580	580	580
E_{sm} (GPa)	186	188	180.7
ε_{sy} (‰)	2.9	2.5	2.6
σ_{sy} (MPa)	540	470	470
ε_{sh} (‰)	32	18.5	18.5
σ_{sh} (MPa)	570	520	520
ε_{su} (‰)	147	133	133
σ_{su} (MPa)	580	580	580
Third branch exponent	1	1	1

LIST OF FIGURE CAPTIONS

Figure 1: Trilinear stress-strain diagram to simulate the fracture mode I crack propagation ($\sigma_{n,2}^{cr} = \alpha_1 \sigma_{n,1}^{cr}$, $\sigma_{n,3}^{cr} = \alpha_2 \sigma_{n,1}^{cr}$, $\varepsilon_{n,2}^{cr} = \xi_1 \varepsilon_{n,u}^{cr}$, $\varepsilon_{n,3}^{cr} = \xi_2 \varepsilon_{n,u}^{cr}$).

Figure 2: Diagrams to simulate the relationship between the crack shear stress and crack shear strain component, and possible shear crack statuses.

Figure 3: Test configuration (All dimensions are in mm).

Figure 4: General information about the beams of the experimental program (CFRP laminates in dashed line).

Figure 5: Monitoring system.

Figure 6: Force *vs.* deflection at the loaded-section for the beams strengthened with the: (a) lowest; (b) intermediate; (c) highest percentage of CFRP shear strengthening.

Figure 7: Finite element mesh of the beam 2S-4LI45 (dimensions are in mm).

Figure 8: Uniaxial constitutive model for the steel bars [7].

Figure 9: Comparison between experimental and numerical force *vs.* deflection at the loaded section relationships.

Figure 10: Crack patterns of the beams (in pink colour: crack completely open; in red colour: crack in the opening process; in cyan colour: crack in the reopening process; in green colour: crack in the closing process; in blue colour: closed crack).

Figure 11: Load *vs.* strains for the beam 2S-4LI45 (a) NSM Laminate A, (b) NSM Laminate B, (c) Steel stirrup.

Figure 12: Details of RC concrete beams: (a) geometry, (b) cross-section of beams with steel stirrups, (c) cross section of beam without steel stirrups, (d) positioning of ~~steel stirrups and~~ CFRP rods in the shear strengthened beams (M8=ϕ8; M10=ϕ11.3; M8=ϕ25.2; dimensions in mm).

Figure 13: Comparison between experimental and numerical relationships between force and deflection at the loaded section for the beams: (a) S0-CON; (b) S0-NSM; (c) S1-CON; (d) S1-NSM.

Figure 14: Influence of $G_{f,s}$ on the: (a) relationship between the force and the deflection at the loaded section, (b)-(d) crack pattern corresponding to the assumed $G_{f,s}$.

Figure 15: Influence of $\tau_{t,p}^{cr}$ on the: (a) relationship between the force and the deflection at the loaded section, (b)-(d) crack pattern corresponding to the assumed $\tau_{t,p}^{cr}$.

Figure 16: Representation of the crack shear stress-shear strain diagram for the $\tau_{t,p}^{cr}$ equal to 0.5, 1.1 and 4.0 MPa.

Figure 17: Influence of β parameter of the $\tau_t^{cr} - \gamma_t^{cr}$ diagram on the relationship between the force and the deflection at the loaded section of beam 2S-4LI45.

Figure 18: Representation of the crack shear stress-crack shear strain diagram for the β equal to 0.05, 0.4 and 0.8.

Figure 19: Influence of using the proposed crack shear softening diagram instead the concept of shear retention factor with $p_1=3$.

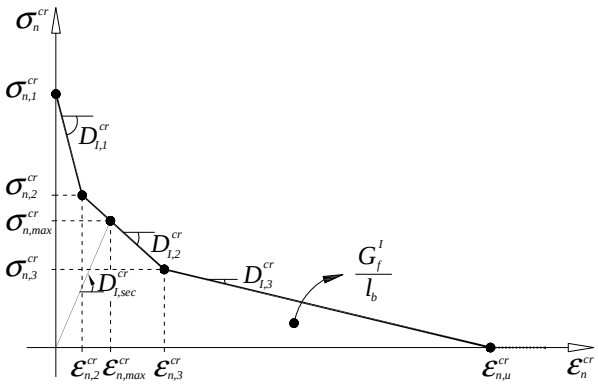

Figure 1: Trilinear stress-strain diagram to simulate the fracture mode I crack propagation ($\sigma_{n,2}^{cr} = \alpha_1 \, \sigma_{n,1}^{cr}$, $\sigma_{n,3}^{cr} = \alpha_2 \, \sigma_{n,1}^{cr}$, $\varepsilon_{n,2}^{cr} = \xi_1 \, \varepsilon_{n,u}^{cr}$, $\varepsilon_{n,3}^{cr} = \xi_2 \, \varepsilon_{n,u}^{cr}$).

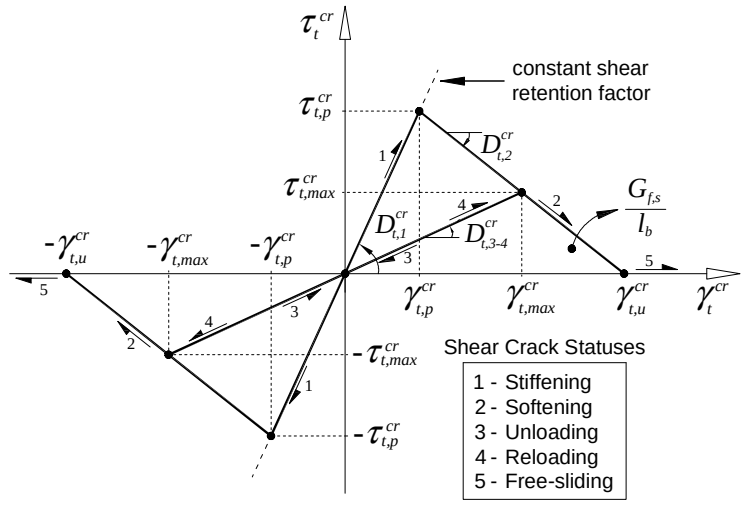

a)

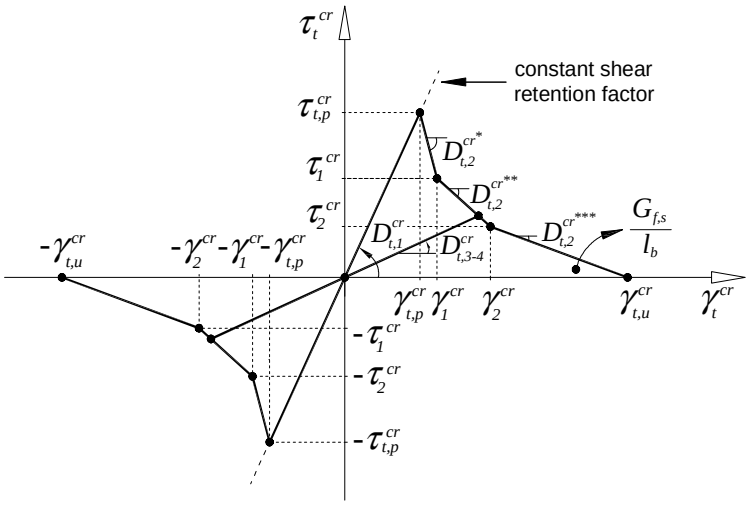

b)

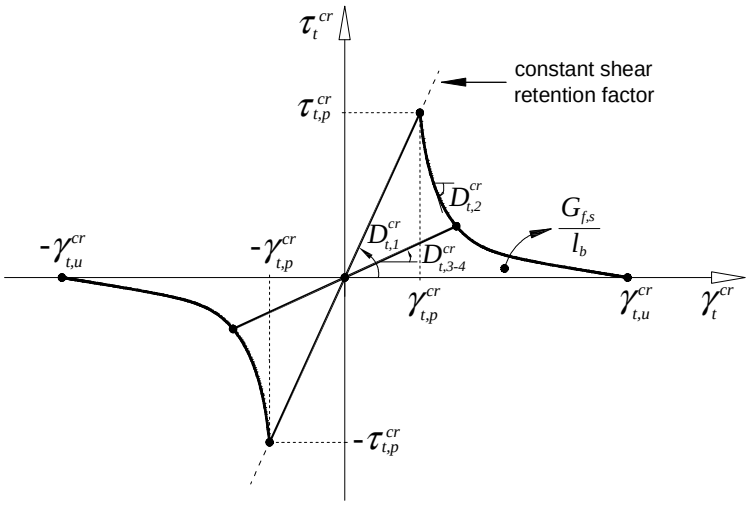

c)

Figure 2: Diagrams to simulate the relationship between the crack shear stress and crack shear strain component, and possible shear crack statuses.

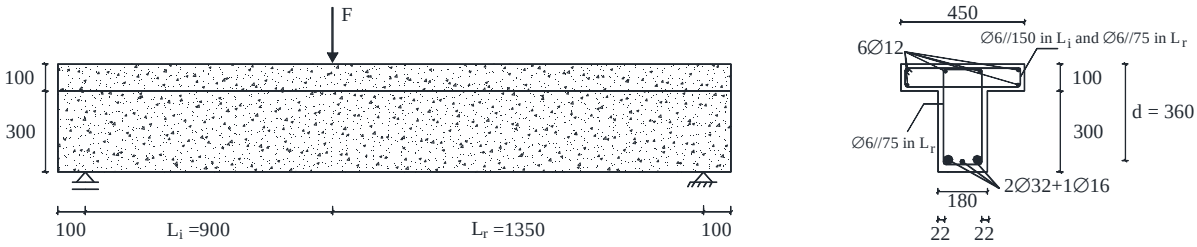

Figure 3: Test configuration (All dimensions are in mm).

Beams ID	Shear strengthening system	Shear strengthening arrangements
2S-R	Reference beam without CFRP	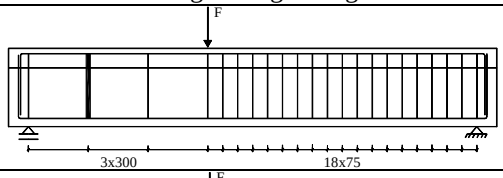
2S-4LV	NSM CFRP laminates at 90° (2 × 4 laminates: ρ_{fw} = 0.08%)	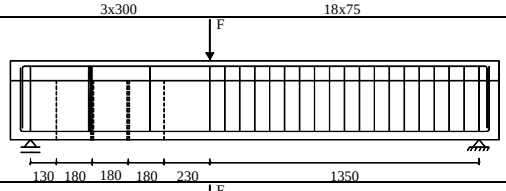
2S-7LV	NSM CFRP laminates at 90° (2 × 7 laminates: ρ_{fw} = 0.13%)	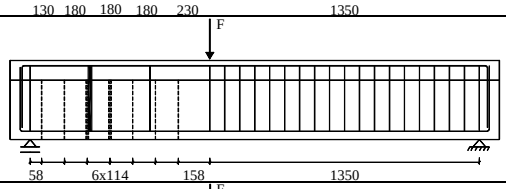
2S-10LV	NSM CFRP laminates at 90° (2 × 10 laminates: ρ_{fw} = 0.18%)	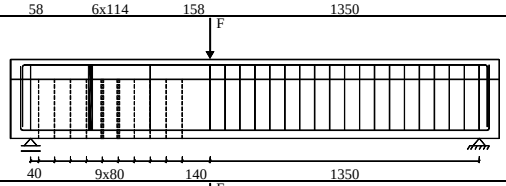
2S-4LI45	NSM CFRP laminates at 45° (2 × 4 laminates: ρ_{fw} = 0.08%)	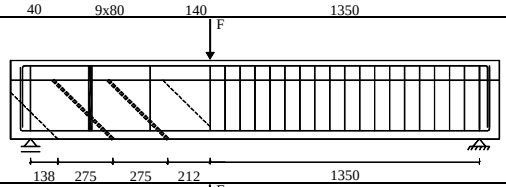
2S-7LI45	NSM CFRP laminates at 45° (2 × 7 laminates: ρ_{fw} = 0.13%)	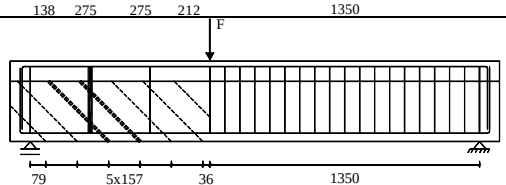
2S-10LI45	NSM CFRP laminates at 45° (2 × 10 laminates: ρ_{fw} = 0.19%)	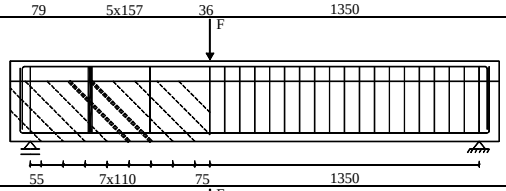
2S-4LI60	NSM CFRP laminates at 60° (2 × 4 laminates: ρ_{fw} = 0.07%)	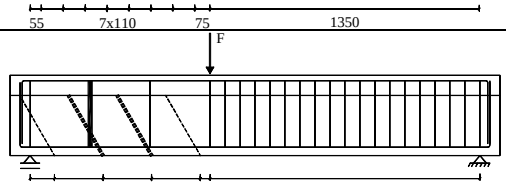
2S-6LI60	NSM CFRP laminates at 60° (2 × 6 laminates: ρ_{fw} = 0.11%)	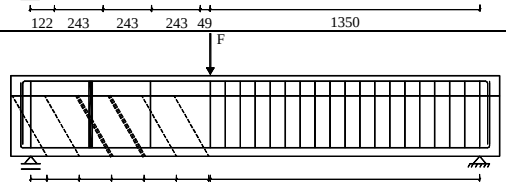
2S-9LI60	NSM CFRP laminates at 60° (2 × 9 laminates: ρ_{fw} = 0.16%)	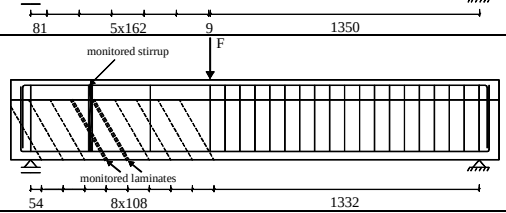
Legend (see exemple in 2S-9LI60 beam): monitored stirrup or or monitored laminate		

Figure 4: General information about the beams of the experimental program (CFRP laminates in dashed line).

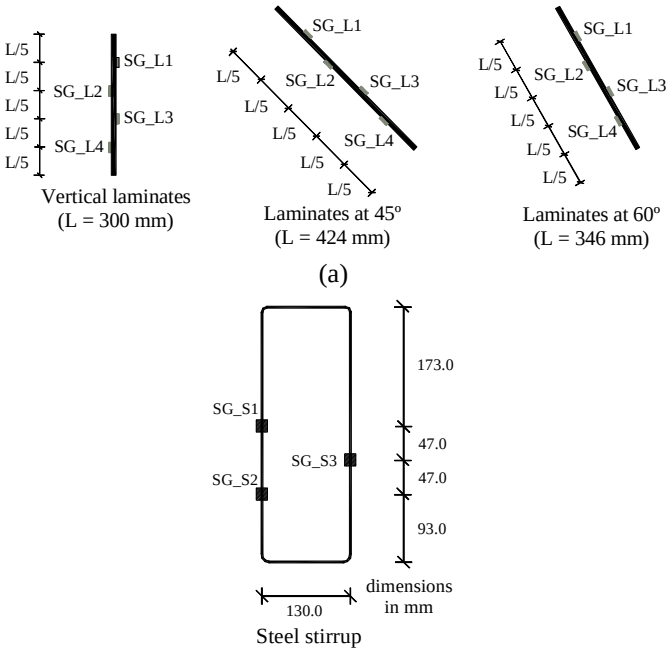

Figure 5: Monitoring system.

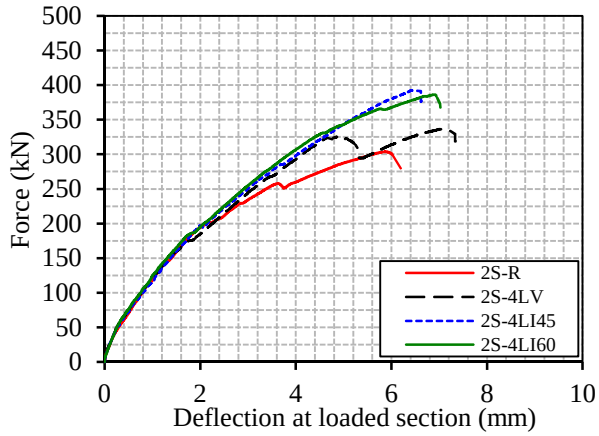

(a)

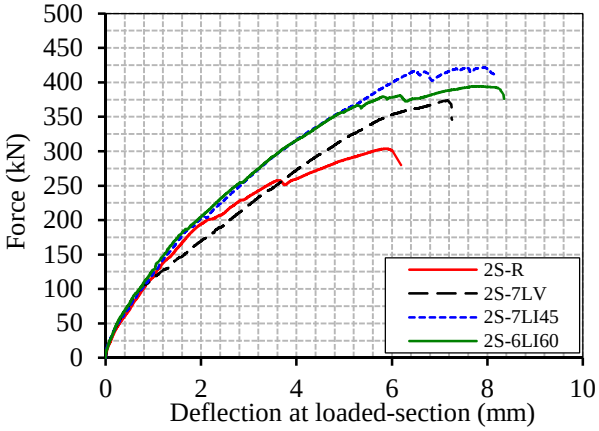

(b)

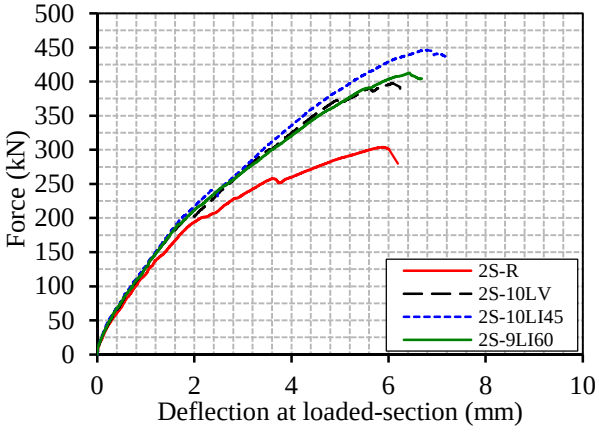

(c)

Figure 6: Force *vs.* deflection at the loaded-section for the beams strengthened with the: (a) lowest; (b) intermediate; (c) highest percentage of CFRP shear strengthening.

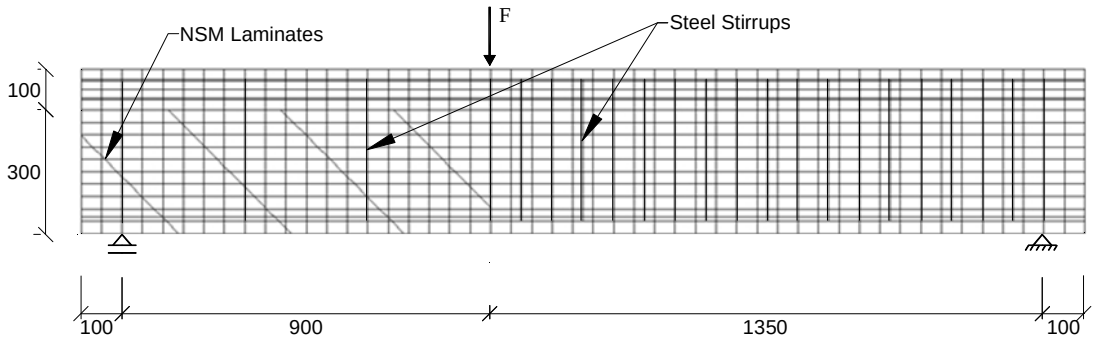

Figure 7: Finite element mesh of the beam 2S-4LI45 (dimensions are in mm).

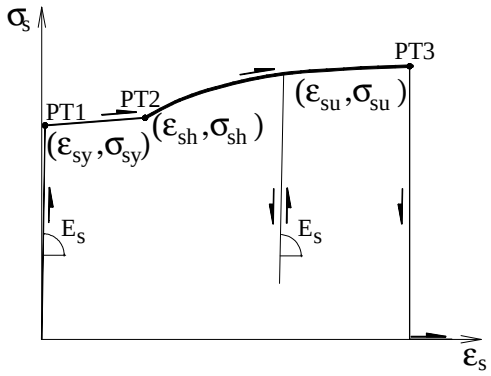

Figure 8: Uniaxial constitutive model for the steel bars [7].

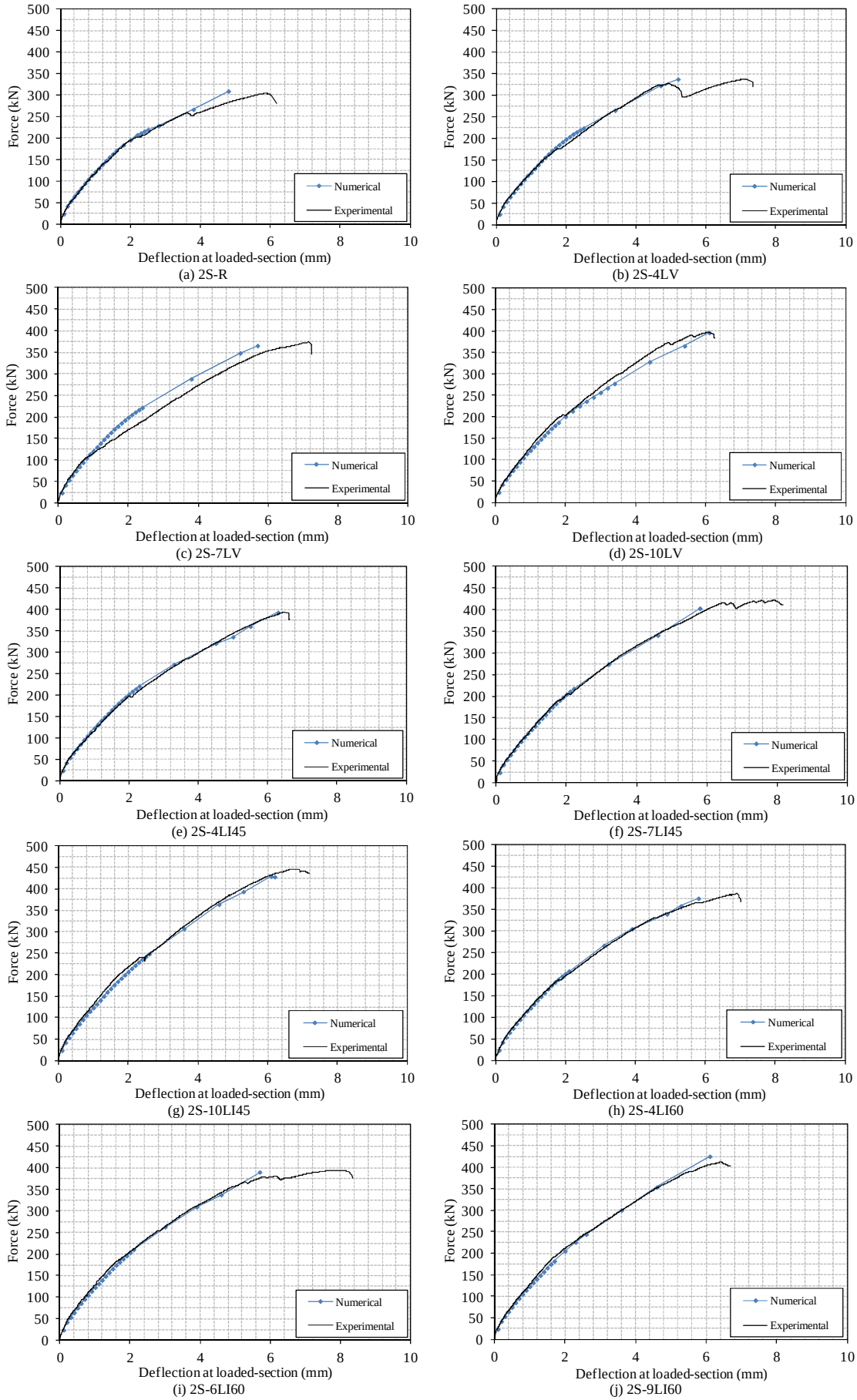

Figure 9: Comparison between experimental and numerical force *vs.* deflection at the loaded section relationships

ID	Experimental Program	Numerical Simulation
2S-R		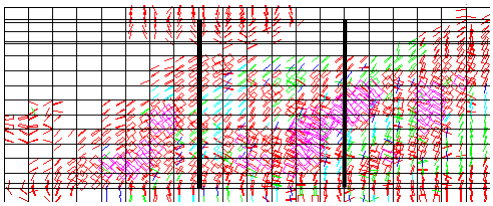
2S-4LV		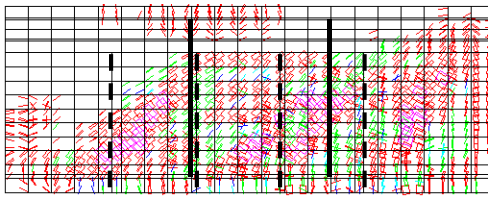
2S-7LV		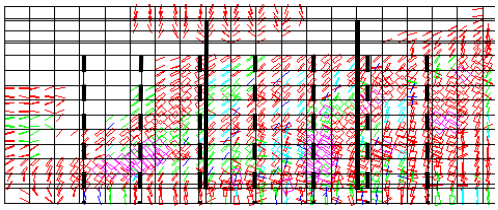
2S-10LV		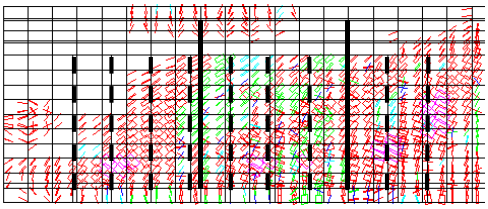
2S-4LI45		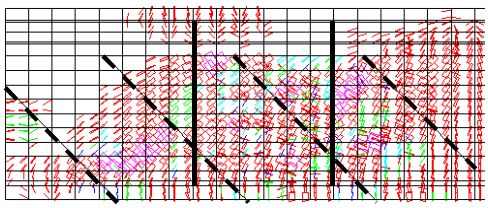
2S-7LI45		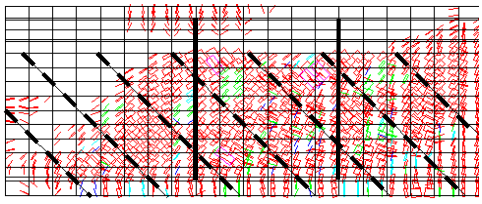
2S-10LI45		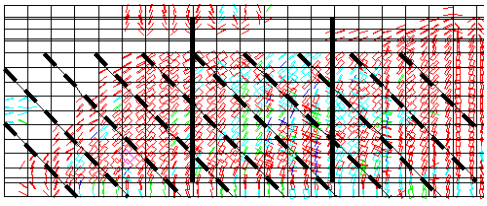
2S-4LI60		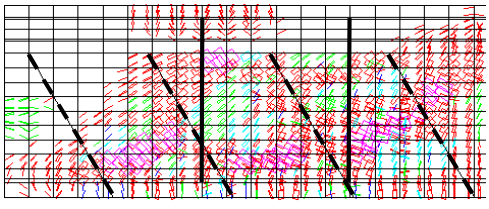

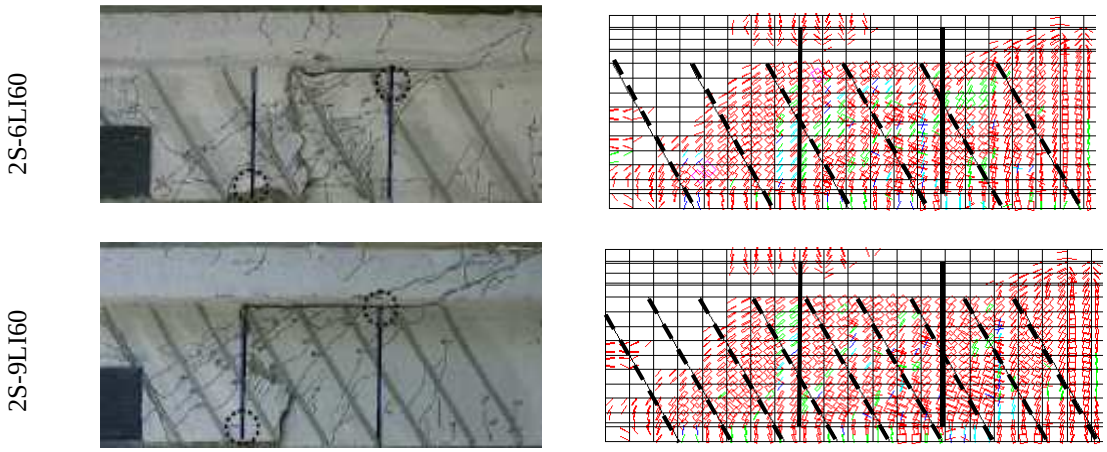

Figure 10: Crack patterns of the beams (in pink colour: crack completely open; in red colour: crack in the opening process; in cyan colour: crack in the reopening process; in green colour: crack in the closing process; in blue colour: closed crack).

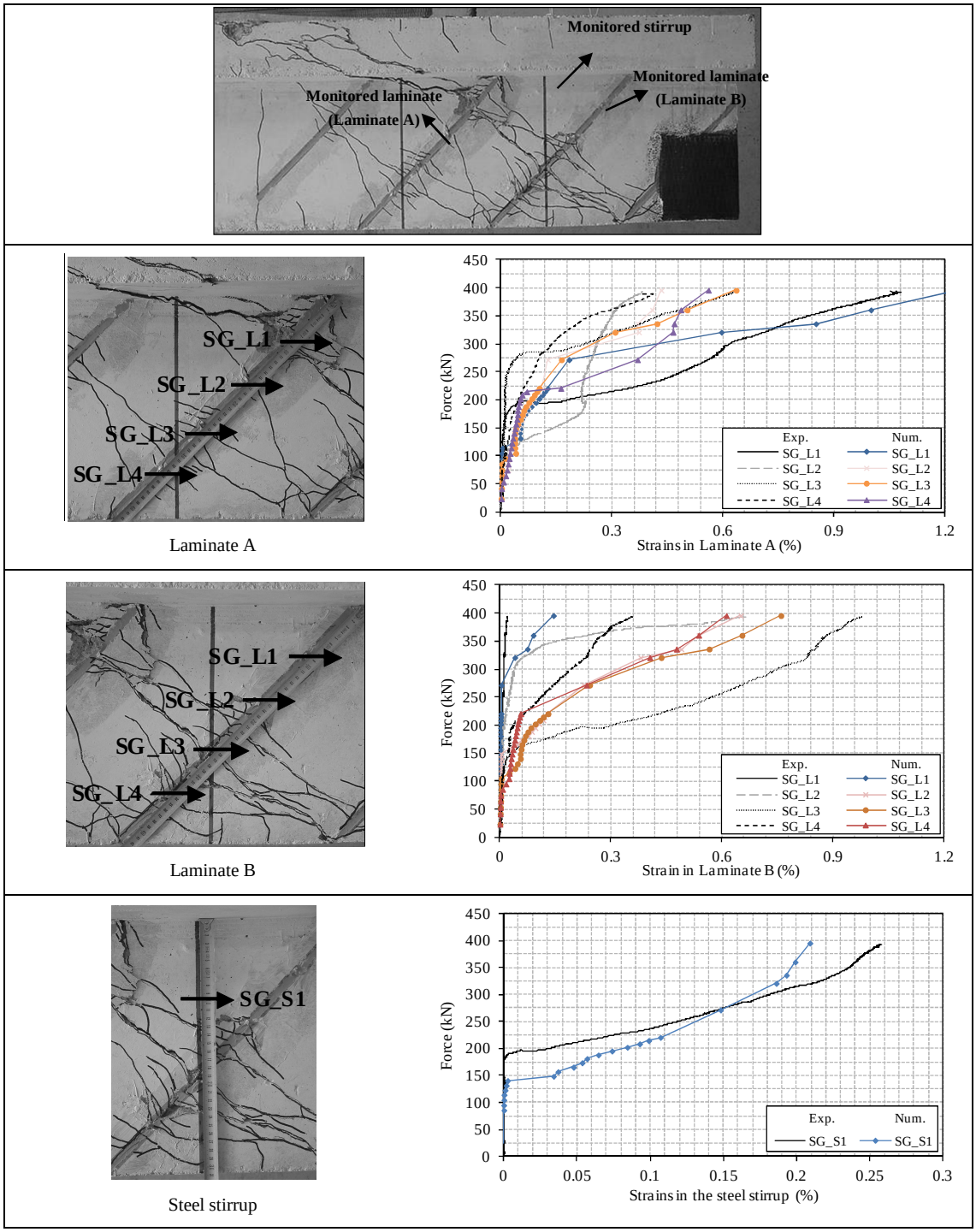

Figure 11: Force *vs* strains for the beam 2S-4LI45 (a) NSM Laminate A, (b) NSM Laminate B, (c) Steel stirrup.

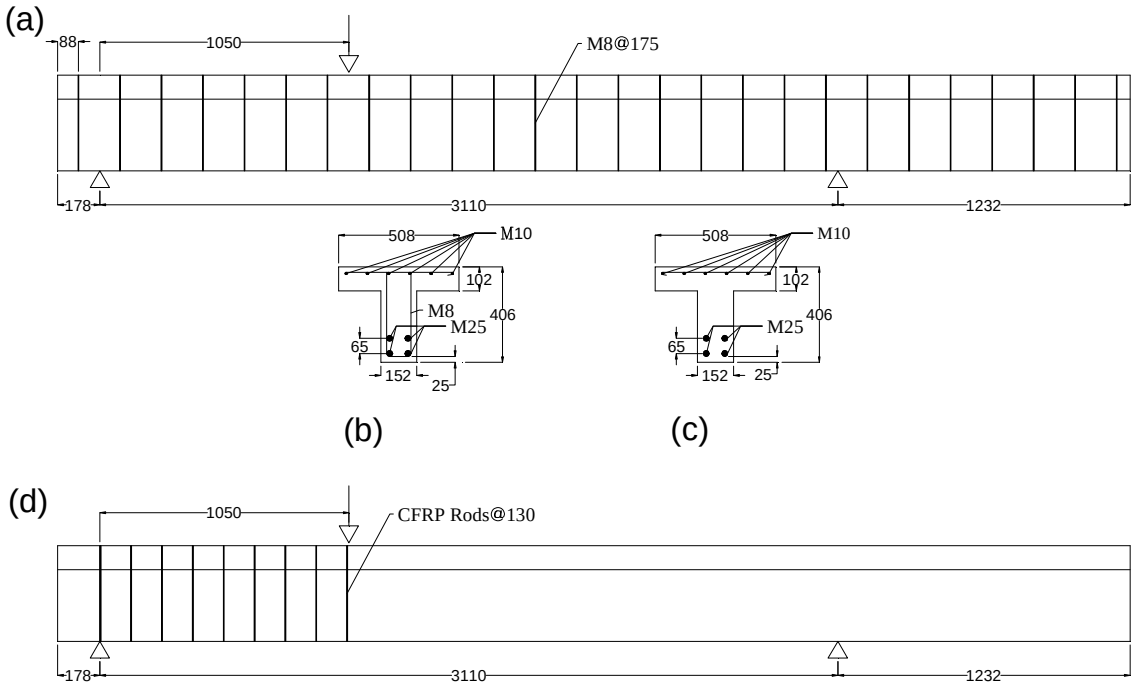

Figure 12: Details of RC concrete beams: (a) geometry, (b) cross-section of beams with steel stirrups, (c) cross section of beam without steel stirrups, (d) positioning of ~~steel stirrups and~~ CFRP rods in the shear strengthened beams (M8=ϕ8; M10=ϕ11.3; M8=ϕ25.2; dimensions in mm).

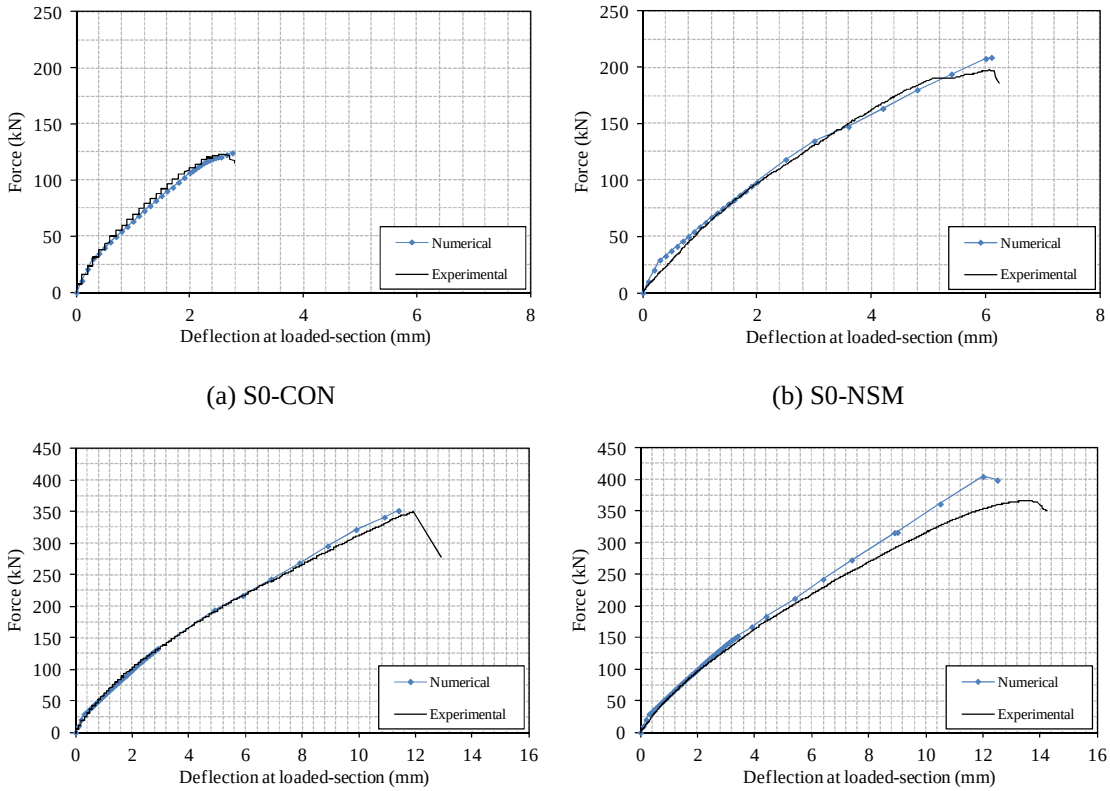

(a) S0-CON (b) S0-NSM

(c) S1-CON (d) S1-NSM

Figure 13: Comparison between experimental and numerical relationships between force and deflection at the loaded section for the beams: (a) S0-CON; (b) S0-NSM; (c) S1-CON; (d) S1-NSM.

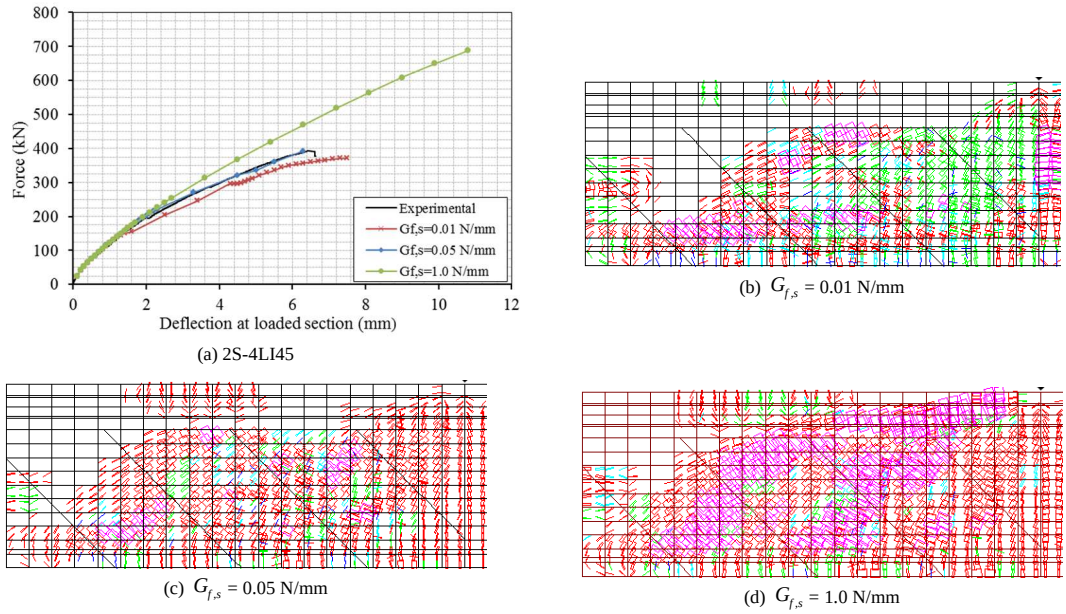

(a) 2S-4LI45

(b) $G_{f,s}$ = 0.01 N/mm

(c) $G_{f,s}$ = 0.05 N/mm

(d) $G_{f,s}$ = 1.0 N/mm

Figure 14: Influence of $G_{f,s}$ on the: (a) relationship between the force and the deflection at the loaded section, (b)-(d) crack pattern corresponding to the assumed $G_{f,s}$.

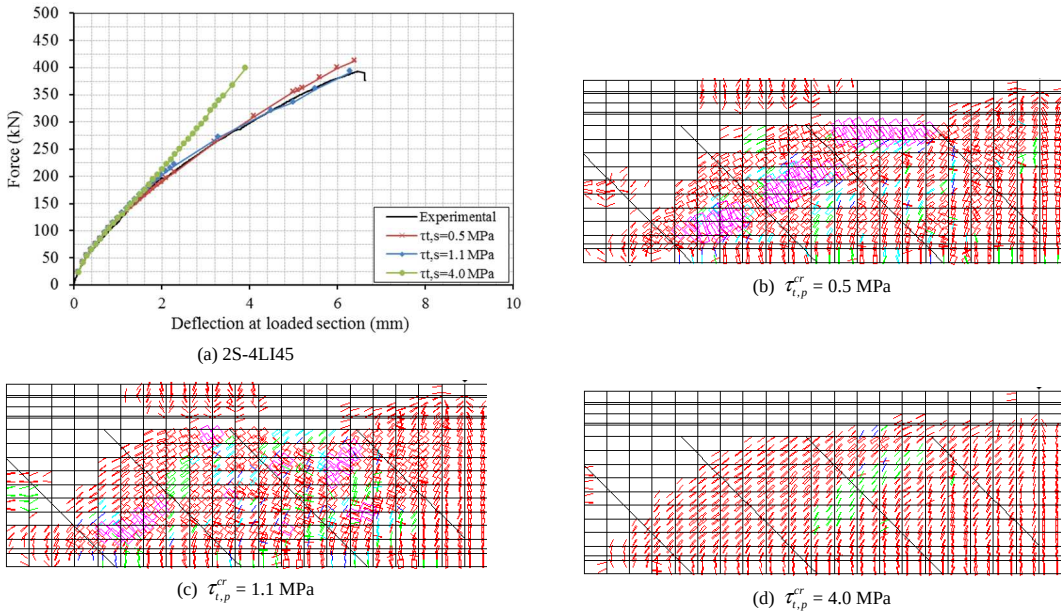

(a) 2S-4LI45

(b) $\tau_{t,p}^{cr}$ = 0.5 MPa

(c) $\tau_{t,p}^{cr}$ = 1.1 MPa

(d) $\tau_{t,p}^{cr}$ = 4.0 MPa

Figure 15: Influence of $\tau_{t,p}^{cr}$ on the: (a) relationship between the force and the deflection at the loaded section, (b)-(d) crack pattern corresponding to the assumed $\tau_{t,p}^{cr}$.

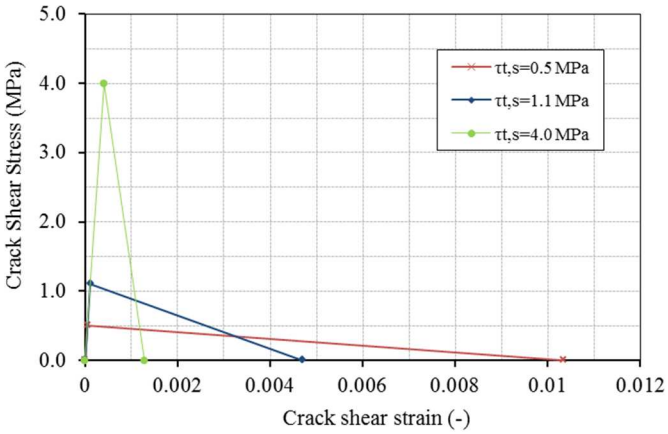

Figure 16: Representation of the crack shear stress-shear strain diagram for the $\tau_{t,p}^{cr}$ equal to 0.5, 1.1 and 4.0 MPa.

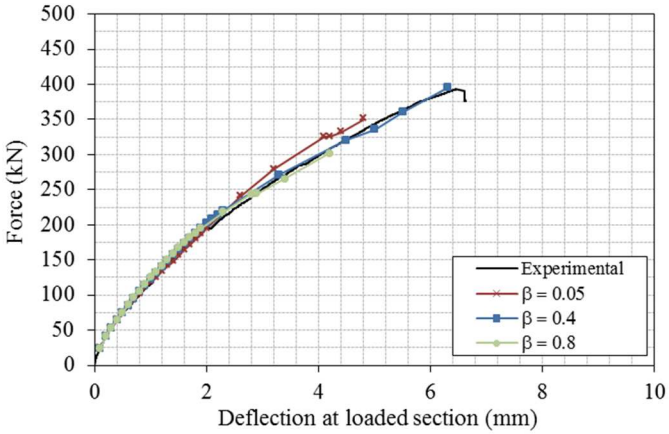

Figure 17: Influence of β parameter of the $\tau_t^{cr} - \gamma_t^{cr}$ diagram on the relationship between the force and the deflection at the loaded section of beam 2S-4LI45.

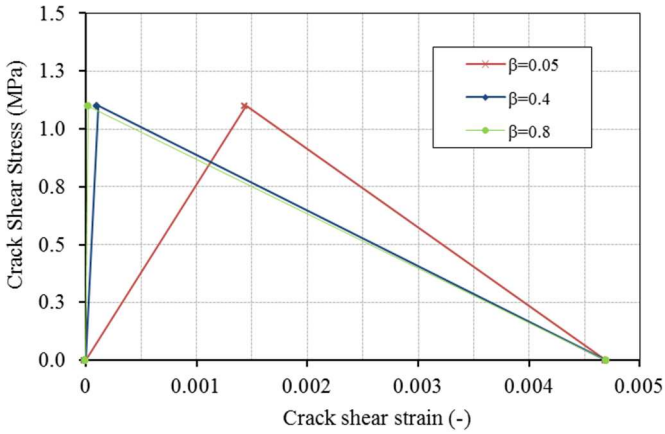

Figure 18: Representation of the crack shear stress-crack shear strain diagram for the β equal to 0.05, 0.4 and 0.8.

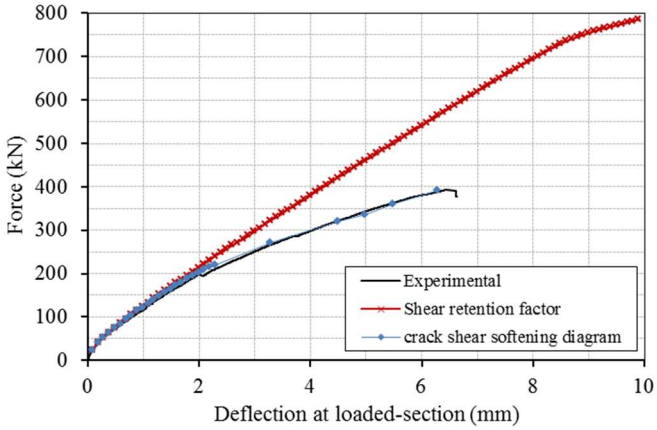

Figure 19: Influence of using the proposed crack shear softening diagram instead the concept of shear retention factor with $p_1=3$.